

## Projected Hartree-Fock and Hartree-Fock-Bogoliubov Spectra for Even Ti, Cr, and Fe Isotopes

Harish Chandra\* and M. L. Rustgi

*Nuclear Physics Laboratory and Department of Physics, State University of New York, Buffalo, New York 14214*

(Received 5 July 1972)

Projection of good angular momentum states has been performed for the deformed self-consistent solutions of even Ti, Cr, and Fe isotopes for the central Yukawa and Kuo-Brown interactions. The results from the two interactions are generally similar though striking dissimilarity in the level spacings is also observed in quite a few cases. The percentage composition of the different angular momentum states in a given deformed solution has been also calculated and compared for both the interactions. The energy spectra, when compared with the known experimental results, are found to agree qualitatively.

### I. INTRODUCTION

In a recent paper by the authors,<sup>1</sup> results of self-consistent Hartree-Fock (HF) and Hartree-Fock-Bogoliubov (HFB) calculations have been reported for even Ti, Cr, and Fe isotopes with an axis of symmetry. These calculations were carried out assuming a <sup>40</sup>Ca spherical core and the extracore nucleons were allowed to interact via two-body central Yukawa and renormalized Kuo-Brown<sup>2</sup> interactions. On the one hand, this study provided useful information on the shapes of the nuclei together with the effect of the pairing term of the Hamiltonian on the structure of the wave function and the binding energy. On the other hand, a comparative study of the microscopic, as well as macroscopic properties of self-consistent solutions for a given isotope, was naturally possible for two entirely different nuclear interactions.

It is well known that the deformed intrinsic wave function corresponding to an axially symmetric shape can be expressed as a superposition of good angular momentum states, and this fact following the pioneering work of Peierls and Yoccoz<sup>3</sup> can be utilized in projecting from the HF wave function the components of good angular momentum states. The spectra obtained from this technique can be directly compared with the observed energy levels. Many such calculations for  $1p$  and  $2s-1d$ -shell nuclei<sup>4-6</sup> have been reported in the literature. However, the mathematical formalism is found to be inadequate when pairing correlations between the nucleons are present. The framework for angular momentum projections from deformed BCS or HFB wave functions has been laid out by Onishi and Yoshida.<sup>7</sup> Using the procedure of Ref. 7 some calculations have been recently reported.<sup>8</sup> In spite of the usefulness of this formalism,<sup>7</sup> its applicability is limited in some practical cases due to the

assumption of partial unoccupation probability in all single-quasiparticle states that make their appearance in the calculation. The necessary modification to the Onishi-Yoshida formalism has been made by Beck, Mang, and Ring,<sup>9</sup> who obtained expressions devoid of any such singularity. In the present work we have used the results of Ref. 9 with suitable modifications.

It may be mentioned that in this paper, for any given isotope, the states with good angular momentum  $J$ , are projected from the intrinsic deformed wave function obtained from the self-consistent HF or HFB calculations reported in Ref. 1, though in principle the projection should precede variation to obtain good angular momentum states with the lowest possible energies.

In Sec. II we give a brief description of the mathematical details used in Refs. 7 and 9 as adopted for our present calculation. The results of the calculations are presented in Sec. III. The calculations have been carried out for the central Yukawa and Kuo-Brown (referred to as HJ interaction in the text, since it is based on the Hamada Johnston potential) interactions. The strengths of the central Yukawa (CY) interaction,

$$V_{ST}(r) = V_{ST}^0 e^{-r/\beta} / (r/\beta), \quad (1)$$

corresponding to the various two-nucleon states are the same as those used in Ref. 1 and are also given below:

$$V_{31}^0 = -46.9 \text{ MeV}, \quad V_{13}^0 = -34.4 \text{ MeV},$$

$$V_{33}^0 = 19.4 \text{ MeV}, \quad V_{11}^0 = 40.9 \text{ MeV}.$$

In Eq. (1)  $S$  and  $T$  denote the multiplicities of the spin and isospin. The range of the interaction,  $\beta$ , is taken to be equal to the Compton wavelength of the pion. The harmonic-oscillator wave functions used to evaluate the two-body matrix elements for

the CY interaction correspond to the oscillator range parameter  $b = 1.96 \times 10^{-13}$  cm, in agreement with the value used by Kuo and Brown. The Kuo-Brown matrix elements used in the calculation are those calculated specifically for the  $0f-1p$  shell. Section IV contains summary and conclusions.

## II. MATHEMATICAL FORMALISM

As mentioned above, the intrinsic wave function corresponding to a deformed shape of the nucleus can be written as

$$|\Phi_K\rangle = \sum_J a_J^K |\Psi_J^K\rangle, \quad (2)$$

where  $K$  is the angular momentum projection quantum number about the axis of symmetry and is zero for an even-even axially symmetric nucleus. Rotating this wave function through an angle  $\Omega$  [ $\Omega$  is an abbreviation for the three Euler angles:  $\Omega \equiv (\alpha, \beta \equiv \theta, \gamma)$ ], we obtain

$$R(\Omega)|\Phi_K\rangle = \sum_{J'} \sum_{M'} a_{J'}^K D_{M'K}^{J'}(\Omega) |\Psi_{M'}^{J'}\rangle, \quad (3)$$

where  $R(\Omega)$  and  $D_{MK}^J$  denote the rotation operator and rotation matrix as defined in Rose.<sup>10</sup> If we now define a projection operator

$$P_{MK}^J = \frac{(2J+1)}{(8\pi^2)} \int D_{MK}^{J*}(\Omega) R(\Omega) d\Omega, \quad (4)$$

such that

$$a_J^K |\Psi_{MK}^J\rangle = P_{MK}^J |\Phi_K\rangle, \quad (5)$$

then on making use of Eq. (4.21) from Rose,<sup>10</sup> for  $K=0$ , one obtains

$$a_J^2 = \frac{(2J+1)}{2} \int_0^\pi d_{00}^J(\theta) \langle \Phi | e^{-i\theta J_y} | \Phi \rangle \sin\theta d\theta. \quad (6)$$

Taking the shell-model Hamiltonian,

$$H = \sum_{\alpha\beta} \langle \alpha | \epsilon | \beta \rangle a_\alpha^\dagger a_\beta + \frac{1}{4} \sum_{\alpha\beta\gamma\delta} \langle \alpha\beta | V_A | \gamma\delta \rangle a_\alpha^\dagger a_\beta^\dagger a_\delta a_\gamma, \quad (7)$$

the energy of a state with angular momentum  $J$

may be obtained from

$$E_J = \frac{\int_0^\pi d_{00}^J(\theta) H(\theta) d(\cos\theta)}{\int_0^\pi d_{00}^J(\theta) N(\theta) d(\cos\theta)}, \quad (8)$$

where

$$H(\theta) = \langle \Phi | H | \Phi(\theta) \rangle \equiv \langle \Phi | H e^{-i\theta J_y} | \Phi \rangle, \quad (9)$$

$$N(\theta) = \langle \Phi | \Phi(\theta) \rangle \equiv \langle \Phi | e^{-i\theta J_y} | \Phi \rangle. \quad (10)$$

Numerical calculations of the integrals in Eq. (8) have been performed by a number of workers.<sup>4-6</sup> However, none of the methods employed in Refs. 4-6 can be applied in the HFB deformed wave functions where the single-quasiparticle states are in general only partially occupied.

In the deformed BCS or HFB<sup>11</sup> state with axial symmetry

$$|\Phi_{\text{BCS}}\rangle = \prod_{\substack{i, m > 0 \\ \tau_z}} (U_m^{i\tau_z} + V_m^{i\tau_z} C_m^{i\tau_z \dagger} C_{\bar{m}}^{i\tau_z \dagger}) |0\rangle, \quad (11)$$

where

$$C_m^{i\tau_z \dagger} = \sum_j c_m^{i\tau_z} a_{jm\tau_z}^\dagger, \quad C_{\bar{m}}^{i\tau_z} = \sum_j c_{\bar{m}}^{i\tau_z} a_{jm\tau_z}. \quad (12)$$

Following Bayman,<sup>12</sup> one can write Eq. (11) as

$$|\Phi_{\text{BCS}}\rangle = N_0 \exp\left(\frac{1}{2} \sum_{\alpha\beta} f_{\alpha\beta} a_\alpha^\dagger a_\beta^\dagger\right) |0\rangle, \quad (13)$$

where

$$f_{\alpha\beta} = \sum_i \frac{V_m^{i\tau_z}}{U_m^{i\tau_z}} c_{i\alpha}^{i\tau_z} c_{i\beta}^{i\tau_z} \delta_{m\beta, -m_\alpha}, \quad (14)$$

and

$$N_0 = \prod_{\substack{i, m > 0 \\ \tau_z}} U_m^{i\tau_z}.$$

In Eq. (11) the summation is taken over all the single-particle states (i.e.,  $|j_\alpha m_\alpha\rangle$  and  $|j_{\alpha\bar{m}_\alpha}\rangle$ ).

Following Onishi and Yoshida<sup>7</sup> it can be shown that

$$N(\theta) = N_0 N'_0 \{ \det[1 + M(\theta)] \}^{1/2}, \quad (15)$$

$$H(\theta) = N(\theta) \left[ \sum_{\alpha\beta} \epsilon_{\alpha\beta} \left( \frac{M(\theta)}{1+M(\theta)} \right)_{\beta\alpha} + \frac{1}{2} \sum_{\alpha\beta\gamma\delta} \langle \alpha\beta | V_A | \gamma\delta \rangle \left( \frac{M(\theta)}{1+M(\theta)} \right)_{\gamma\alpha} \left( \frac{M(\theta)}{1+M(\theta)} \right)_{\delta\beta} \right. \\ \left. + \frac{1}{4} \sum_{\alpha\beta\gamma\delta} \langle \alpha\beta | V_A | \gamma\delta \rangle \sum_{\rho\nu} \left( \frac{1}{1+M(\theta)} \right)_{\nu\alpha} f_{\nu\beta} \left( \frac{1}{1+M(\theta)} \right)_{\gamma\rho} f'_{\rho\delta} \right], \quad (16)$$

$$f'_{\gamma\delta}(\theta) = \sum_{m'_\gamma m'_\delta} f_{j_\gamma m'_\gamma, j_\delta m'_\delta} d_{m'_\gamma m'_\delta}^{j_\gamma j_\delta}(\theta) d_{m_\delta m_\delta}^{j_\delta j_\delta}(\theta), \quad (17)$$

where

$$M_{\alpha\beta}(\theta) = -\sum_{\gamma} f'_{\alpha\gamma}(\theta) f_{\gamma\beta}. \quad (18)$$

As pointed out earlier, the matrices  $f$  and  $M(\theta)$  become singular in the HF limit. In order to avoid the situation, following Beck, Mang, and Ring,<sup>9</sup> one can introduce the quasiparticle operator

$$A_i^{\dagger} = \sum_{\beta} (\bar{u}_{\beta i} a_{\beta}^{\dagger} + \bar{v}_{\beta i} a_{\beta}), \quad (19)$$

where the charge indices have been suppressed, the summation over  $\beta$  includes the time reversed states and  $\bar{u}$  and  $\bar{v}$  are given by

$$\bar{u} = \bar{c} \bar{U} = \begin{pmatrix} c & 0 \\ 0 & c \end{pmatrix} \begin{pmatrix} U & 0 \\ 0 & U \end{pmatrix}, \quad (20a)$$

$$\bar{v} = \bar{c} \bar{V} = \begin{pmatrix} c & 0 \\ 0 & c \end{pmatrix} \begin{pmatrix} 0 & V \\ -V & 0 \end{pmatrix}. \quad (20b)$$

The above equations enable one to write Eq. (14) and  $N_0 N'_0$  in Eq. (15) as

$$f = \bar{c} \bar{U}^{-1} \bar{V} \bar{c}, \quad (21)$$

$$f'(\theta) = \bar{c}(\theta) \bar{U}^{-1}(\theta) \bar{V}(\theta) \bar{c}(\theta), \quad (22)$$

and

$$N_0 N'_0 = \prod_{i, m > 0} U_m^i U_m^i(\theta) = [\det \bar{U} \det \bar{U}(\theta)]^{1/2}. \quad (23)$$

Employing Eq. (22) it can be seen that

$$N(\theta) = \{ \det[\bar{c}(\theta) \bar{c}] \det[\bar{u}(\theta) \bar{u} + \bar{v}(\theta) \bar{v}] \}^{1/2} \\ \equiv [\det K(\theta)]^{1/2}, \quad (24)$$

where

$$K(\theta) = \bar{u}(\theta) \bar{u} + \bar{v}(\theta) \bar{v}.$$

On employing the antisymmetric property of  $f'(\theta)$  it is easy to show that

$$\bar{\rho}(\theta) = \frac{M(\theta)}{1+M(\theta)} = \bar{v}(\theta) \bar{K}^{-1}(\theta) \bar{v}, \quad (25a)$$

$$\chi(\theta) = \frac{1}{1+M(\theta)} f'(\theta) = \bar{u} K^{-1}(\theta) \bar{v}(\theta), \quad (25b)$$

$$\bar{\chi}(\theta) = \left( \frac{1}{1+M(\theta)} \right) f = -\bar{v} K^{-1}(\theta) \bar{u}(\theta). \quad (25c)$$

The matrices  $\chi(\theta)$  and  $\bar{\chi}(\theta)$  are antisymmetric and  $\bar{K}^{-1}(\theta)$  is the transpose of  $K^{-1}(\theta)$ . In terms of  $\rho(\theta)$ ,  $\chi(\theta)$ , and  $\bar{\chi}(\theta)$ , we can write  $H(\theta)$  after introducing the isospin quantum numbers and ultimately  $E(\theta)$  as

$$E(\theta) = \frac{H(\theta)}{N(\theta)} = \sum_{\alpha\tau_z} \epsilon_{\alpha\tau_z}^{\tau_z} \rho_{\alpha\alpha}^{\tau_z}(\theta) + \sum_{\tau_z} \text{Tr}^{\tau_z} [\Gamma(\theta) \bar{\rho}(\theta)]_{\tau_z} \\ + \frac{1}{2} \sum_{\tau_z} \text{Tr}^{\tau_z} [\Delta(\theta) \bar{\chi}(\theta)]_{\tau_z}, \quad (26a)$$

where

$$\Gamma_{\alpha\gamma}^{\tau_z}(\theta) = \frac{1}{2} \sum_{\beta\tau_z, \delta} \langle \alpha\tau_z \beta\tau_z' | V_A | \gamma\tau_z \delta\tau_z' \rangle \rho_{\beta\delta}^{\tau_z}(\theta), \quad (26b)$$

and

$$\Delta_{\alpha\beta}^{\tau_z}(\theta) = \frac{1}{2} \sum_{\gamma\delta} \langle \alpha\tau_z \beta\tau_z | V_A | \gamma\tau_z \delta\tau_z \rangle \chi_{\gamma\delta}^{\tau_z}(\theta). \quad (26c)$$

In the limit  $\theta \rightarrow 0$ ,  $E(\theta) \rightarrow H(\theta)$ , and  $N(\theta) \rightarrow 1$ . Having obtained the values of  $H(\theta)$  and  $N(\theta)$  for different values of  $\theta$ , one can obtain  $E_J$  and  $a_j^2$  by making use of Eqs. (8) and (6), respectively. The rotated BCS wave function which is needed in the evaluation of  $H(\theta)$  and  $N(\theta)$  is given by

$$|\Phi_{\text{BCS}}(\theta)\rangle = e^{-i\theta J_y} |\Phi_{\text{BCS}}\rangle = \prod_i A_i(\theta) |0\rangle, \quad (27)$$

where

$$A_i^{\dagger}(\theta) = e^{-i\theta J_y} A_i^{\dagger} e^{i\theta J_y}. \quad (28)$$

On employing Eq. (19) in Eq. (28) and introducing a complete set of eigenfunctions, it is found that

$$A_i^{\dagger}(\theta) = \sum_{\beta} \{ [\bar{u}(\theta)]_{\beta i} a_{\beta}^{\dagger} + [\bar{v}(\theta)]_{\beta i} a_{\beta} \}, \quad (29)$$

where

$$\bar{u}(\theta) = R(\theta) \bar{u} \text{ and } \bar{v}(\theta) = R(\theta) \bar{v}. \quad (30)$$

The matrix  $R(\theta)$  is the familiar  $d_{mm'}^j(\theta)$  matrix as given in Ref. 10.

### III. NUMERICAL RESULTS

#### A. Procedure for the Calculation

Calculation of  $E_J$  and  $a_j^2$  is made possible from a given intrinsic deformed wave function with the help of Eqs. (8) and (6) of the previous section. It is evident from the structure of integrals in Eqs. (6) and (8) that they are in general not analytically integrable. The numerical procedure of 16-point Gaussian quadrature, with points distributed in the integration range from  $\beta(\equiv \theta) = 0$  to  $\pi$  and symmetric about  $\pi/2$ , is therefore employed in evaluating them. In a few cases the results were checked with the 32-point quadrature and were not found to be different except in the  $J=8$  state. The computer time was also saved by realizing that for axially symmetric even-even nuclei,

$$N(\beta) = N(\pi - \beta), \quad H(\beta) = H(\pi - \beta). \quad (31)$$

Since  $\sin\beta$  and  $d_{00}^J(\beta)$  are symmetrical about  $\frac{1}{2}\pi$ ,  $N(\beta)$  and  $H(\beta)$  were calculated only for those 8 points of the 16-point quadrature which fall between 0 and  $\frac{1}{2}\pi$ . In the beginning of the calculations, however, the computer program was checked for symmetry by calculating  $N(\beta)$  and  $H(\beta)$  for all the 16 points.

TABLE I. Values of  $N(\beta) = \langle \Phi | e^{-i\beta J_y} | \Phi \rangle$  and  $H'(\beta) = \langle \Phi | \text{He}^{-i\beta J_y} | \Phi \rangle / \langle \Phi | H | \Phi \rangle$  for  $^{48}\text{Ti}$ ,  $^{50}\text{Cr}$ , and  $^{58}\text{Fe}$  prolate HFB solutions along with the oblate solution for  $^{58}\text{Fe}$ , all corresponding to the CY interaction. Since  $N(\beta)$  and  $H'(\beta)$  are symmetrical about  $90^\circ$ , only the values between  $0$  and  $90^\circ$  are given.

$\beta$ in degrees	$^{48}\text{Ti}$		$^{50}\text{Cr}$		$^{58}\text{Fe}$ (Prolate)		$^{58}\text{Fe}$ (Oblate)	
	$N(\beta)$	$H'(\beta)$	$N(\beta)$	$H'(\beta)$	$N(\beta)$	$H'(\beta)$	$N(\beta)$	$H'(\beta)$
0.9511	0.998 420	0.998 590	0.997 886	0.998 121	0.998 956	0.999 053	0.998 741	0.998 854
4.9904	0.955 526	0.957 124	0.946 540	0.947 221	0.966 403	0.966 520	0.962 634	0.962 761
12.0951	0.765 490	0.772 648	0.724 867	0.727 220	0.817 994	0.818 186	0.800 454	0.800 588
22.0129	0.415 114	0.428 086	0.346 486	0.350 299	0.518 531	0.518 779	0.487 274	0.487 152
34.3888	0.124 250	0.133 883	0.077 879	0.080 265	0.211 575	0.211 720	0.192 500	0.191 829
48.7757	0.031 616	0.036 096	0.006 710	0.007 262	0.053 163	0.053 197	0.055 543	0.054 772
64.6580	0.027 559	0.031 525	0.000 266	0.000 350	0.010 371	0.010 393	0.019 103	0.018 595
81.4514	0.017 053	0.019 927	0.000 165	0.000 204	0.003 098	0.003 124	0.011 601	0.011 238

### B. Applicability of the Projection Technique

Tables I and II show the values of  $N(\beta \equiv \theta)$  and  $H(\beta \equiv \theta)$  as a function of  $\beta$  (in degrees) for  $^{48}\text{Ti}$ ,  $^{50}\text{Cr}$ , and  $^{58}\text{Fe}$  for the CY and HJ interactions, respectively. For  $^{58}\text{Fe}$  the results for both prolate, as well as oblate shapes, are given. In order to see the behavior of  $H(\beta)$  in comparison with  $N(\beta)$ , the values of  $H(\beta)$  given in the tables have been divided by the self-consistent energy  $\langle \Phi_{\text{BCS}} | H | \Phi_{\text{BCS}} \rangle$ , and will be referred to as  $H'(\beta)$ .

A comparison of  $H'(\beta)$  thus obtained with  $N(\beta)$  shows that for a given  $\beta$ , these values are very similar. However, their dissimilarity is reflected in a pronounced way if we consider  $H'(\beta)/N(\beta)$ , i.e.,  $E(\beta)$  of Eq. (26a) divided by  $\langle \Phi_{\text{BCS}} | H | \Phi_{\text{BCS}} \rangle$ . The quantity  $E'(\beta)$  thus obtained is plotted as a function of  $\beta$  for all the isotopes mentioned above in Figs. 1 and 2 for the CY and HJ interactions. Since the curves are symmetrical about  $\frac{1}{2}\pi$ , only the values between  $0$  and  $90^\circ$  are plotted. As will be seen later in this section, for a given isotope, the difference in the energy spectrum for the CY and HJ interactions arise mainly due to the structure of these curves. For the present, however, the salient features of these curves will be discussed.

From the figures it is clear that these curves for  $E'(\beta)$  can be classified into three groups. Those for which  $E'(\beta) \geq 1$  fall in the first group and the curves for  $^{48}\text{Ti}$  and  $^{50}\text{Cr}$  belong to this group. The projected energy for the  $J=0$  state ( $E_{J=0}$ ) for a wave function having this characteristic is found to be considerably below the self-consistent energy minimum  $\langle \Phi_{\text{BCS}} | H | \Phi_{\text{BCS}} \rangle$ . This is so because for  $J=0$ ,  $d_{00}^{J=0} = 1$ , and Eq. (8) reduces to

$$E_{J=0} = E_{\text{BCS}} \frac{\int_0^\pi H'(\beta) d(\cos\beta)}{\int_0^\pi N(\beta) d(\cos\beta)}. \quad (32)$$

Since  $H'(\beta)$  and  $N(\beta)$  both decrease with increase in  $\beta$  with  $N(\beta)$  decreasing somewhat faster than  $H'(\beta)$ , it follows that  $\int_0^\pi H'(\beta) d(\cos\beta) / \int_0^\pi N(\beta) d(\cos\beta) > 1$ , giving  $E_{J=0} > E_{\text{BCS}}$ . Since both the energies are negative, the  $J=0$  state will lie below the self-consistent energy minimum. For higher  $J$  states, the variation of  $d_{00}^J(\beta)$  with  $\beta$  decreases the numerator in Eq. (8) more than the denominator resulting in the higher  $J$  values lying above the  $J=0$  state. Thus for  $E'(\beta) \geq 1$ , the projection technique is expected to give meaningful results.

The second group for which  $E'(\beta) = 1$  can be divided into two categories on the basis of the

TABLE II. Values of  $N(\beta) = \langle \Phi | e^{-i\beta J_y} | \Phi \rangle$  and  $H'(\beta) = \langle \Phi | \text{He}^{-i\beta J_y} | \Phi \rangle / \langle \Phi | H | \Phi \rangle$  for  $^{44}\text{Ti}$ ,  $^{50}\text{Cr}$ , and  $^{58}\text{Fe}$  prolate HFB solutions along with the oblate solution for  $^{58}\text{Fe}$  for the KBRME for the HJ interaction. Since  $N(\beta)$  and  $H'(\beta)$  are symmetrical about  $90^\circ$ , only the values between  $0$  and  $90^\circ$  are given.

$\beta$ in degrees	$^{44}\text{Ti}$		$^{50}\text{Cr}$		$^{58}\text{Fe}$ (Prolate)		$^{58}\text{Fe}$ (Oblate)	
	$N(\beta)$	$H'(\beta)$	$N(\beta)$	$H'(\beta)$	$N(\beta)$	$H'(\beta)$	$N(\beta)$	$H'(\beta)$
0.9511	0.997 830	0.997 825	0.997 497	0.997 506	0.998 441	0.998 509	0.998 274	0.998 355
4.9904	0.942 583	0.945 802	0.933 434	0.934 490	0.951 611	0.952 386	0.954 653	0.954 787
12.0951	0.703 955	0.719 353	0.666 606	0.671 212	0.747 035	0.750 467	0.762 443	0.762 744
22.0129	0.302 100	0.327 731	0.259 548	0.265 733	0.384 563	0.390 378	0.412 612	0.412 893
34.3888	0.045 762	0.058 507	0.036 673	0.038 942	0.103 451	0.107 204	0.124 216	0.124 138
48.7757	0.002 509	0.003 707	0.001 332	0.001 503	0.013 571	0.014 486	0.020 284	0.020 130
64.6580	0.002 229	0.003 717	0.000 013	0.000 015	0.001 232	0.001 346	0.002 607	0.002 550
81.4514	0.001 065	0.001 659	0.000 003	0.000 003	0.000 205	0.000 225	0.000 611	0.000 590

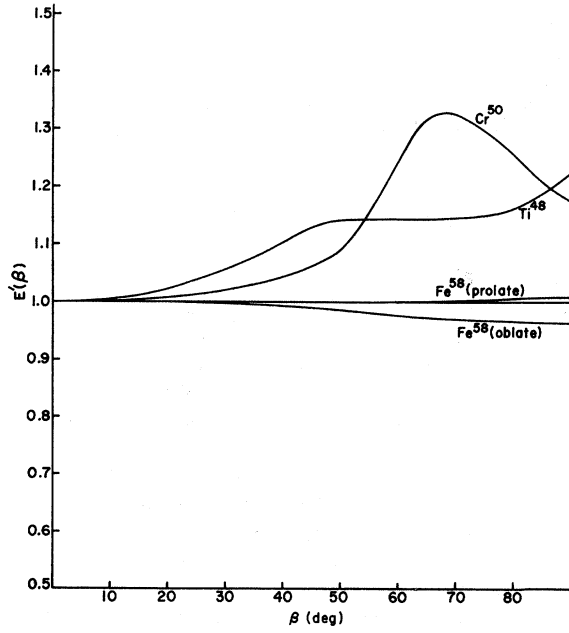


FIG. 1. Plot of  $E'(\beta)$  vs  $\beta$  for  $^{48}\text{Ti}$ ,  $^{50}\text{Cr}$ , and  $^{58}\text{Fe}$  isotopes using the CY interaction.

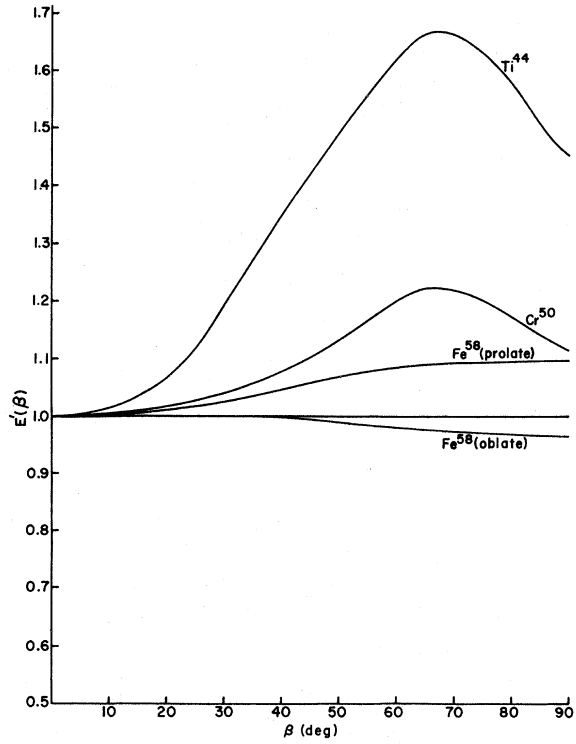


FIG. 2. Plot of  $E'(\beta)$  vs  $\beta$  for  $^{44}\text{Ti}$ ,  $^{50}\text{Cr}$ , and  $^{58}\text{Fe}$  isotopes using the HJ interaction.

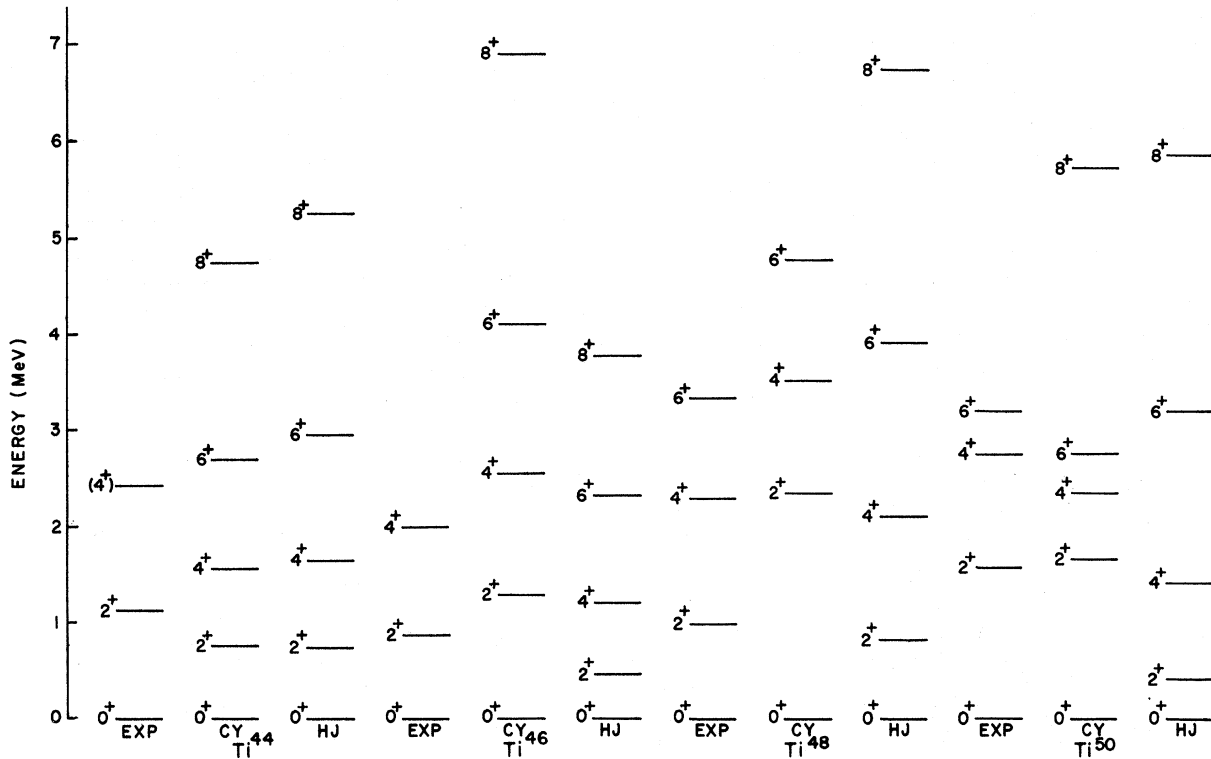


FIG. 3. Comparison of experimental (EXP) [see C. Lederer, J. Hollander, and I. Perlman, *Table of Isotopes* (Wiley, New York, 1967)] and calculated spectra of even Ti isotopes for the CY and HJ interactions.

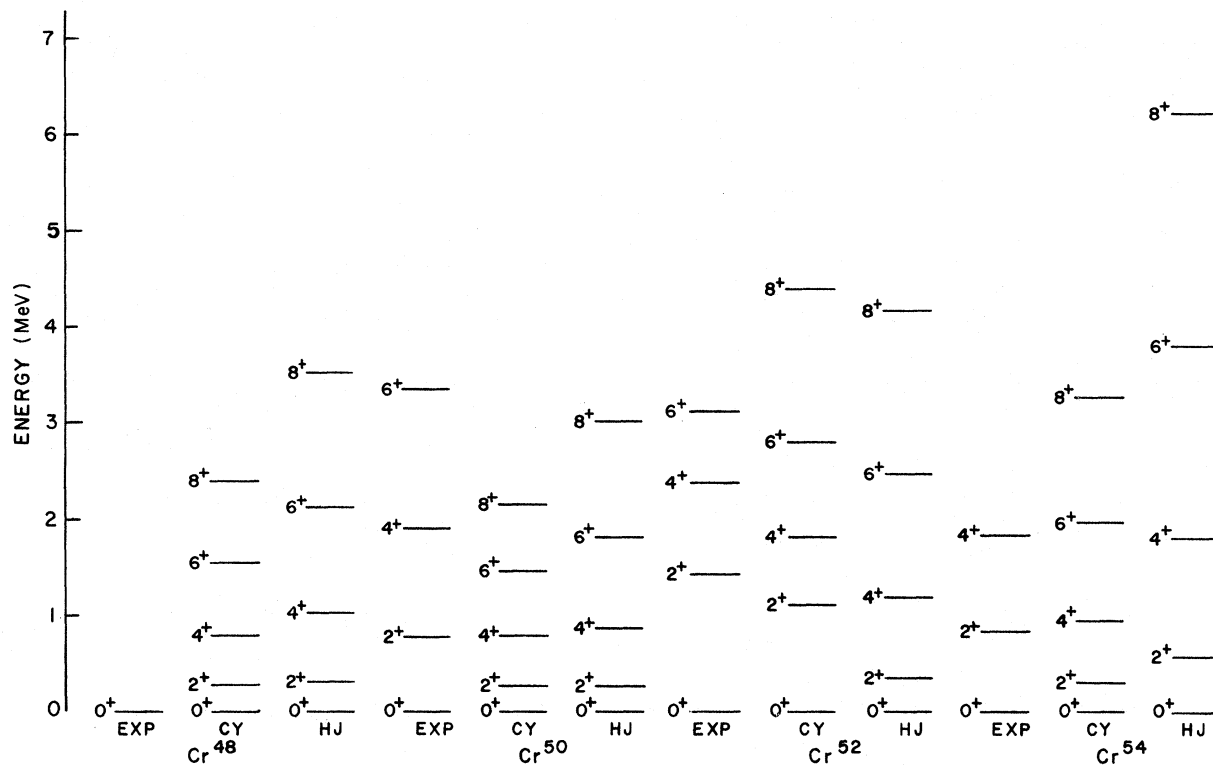


FIG. 4. Comparison of experimental (EXP) [see C. Lederer, J. Hollander, and I. Perlman, *Table of Isotopes* (Wiley, New York, 1967)] and calculated spectra of even Cr isotopes for the CY and HJ interactions.

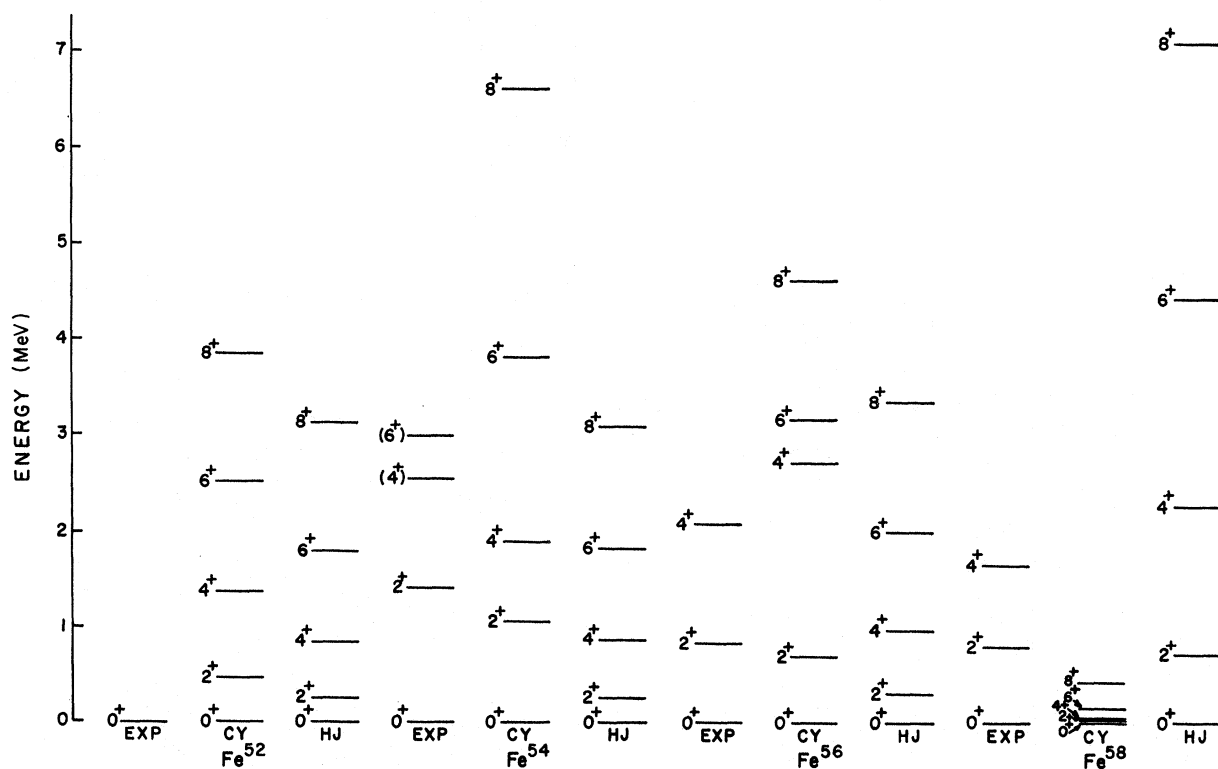


FIG. 5. Comparison of experimental (EXP) [see C. Lederer, J. Hollander, and I. Perlman, *Table of Isotopes* (Wiley, New York, 1967)] and calculated spectra of even Fe isotopes for the CY and HJ interactions.

TABLE III. Calculated self-consistent energy ( $E = \langle \Phi | H | \Phi \rangle$ ), ground-state energy with respect to  $E$ , i.e., ( $E_{J=0} - E$ ), and the percentage distribution of the angular momentum ( $a_J^2$ ) in the deformed intrinsic states of even Ti, Cr, and Fe isotopes for the CY interaction. All the energies are given in MeV. The numbers in the parentheses correspond to the spherical BCS solution.

Isotope	Type of wave function $\Phi$	$\langle \Phi   H   \Phi \rangle = E$	$\Delta E = E_{J=0} - E$	Percentage of $a_J^2$ in the wave function $\Phi$				
				$J=0$	$J=2$	$J=4$	$J=6$	$J=8$
<sup>44</sup> Ti	HF(P)	-28.140	-2.178	5.883	24.339	29.627	22.956	11.955
<sup>46</sup> Ti	HFB(P)	-48.740	-2.959	7.513	28.219	30.842	20.812	9.037
<sup>48</sup> Ti	HFB(P)	-68.430	-3.649	9.824	30.390	30.826	19.881	6.631
<sup>50</sup> Ti	HF(P)	-87.110 (-87.49)	-2.142	15.018	28.581	28.469	21.549	4.192
<sup>48</sup> Cr	HFB(P)	-59.580	-1.150	5.839	24.510	29.319	22.180	11.886
<sup>50</sup> Cr	HFB(P)	-82.160	-0.981	6.868	27.746	30.602	20.631	9.717
<sup>52</sup> Cr	HF(P)	-102.980 (-103.88)	-1.428	14.207	42.920	31.129	9.202	2.077
<sup>54</sup> Cr	HFB(P)	-124.120	-1.409	6.351	26.228	30.260	21.580	10.686
<sup>52</sup> Fe	HFB(P)	-94.630	-1.076	11.299	40.220	32.484	12.945	2.731
<sup>54</sup> Fe	HF(P)	-118.830 (-119.66)	-1.041	22.792	56.436	18.852	1.846	0.096
<sup>56</sup> Fe	HFB(P)	-141.540	-1.762	9.121	33.556	31.384	17.028	6.524
<sup>58</sup> Fe	HFB(P)	-162.260	-0.092	11.490	39.007	31.047	13.660	3.910
<sup>58</sup> Fe	HFB(O)	-161.570	...	...	...	...	...	...

behavior of  $N(\beta)$ . For a deformed intrinsic shape  $N(\beta)$  decreases with increase of  $\beta$  from 0 to  $\frac{1}{2}\pi$ . It can be seen from Eq. (8) that in such a case, the projected spectrum will be degenerate with the self-consistent energy minimum, with each angular momentum state  $J$  having different composition mixture  $a_J^2$  in the deformed wave function. In the strict sense such a case was not confronted in the present calculation though <sup>58</sup>Fe (prolate) for

the CY interaction (Fig. 1) comes quite close to it. In the second category of this group fall those isotopes which have a spherical shape. For such cases,  $E'(\beta)$  and  $N(\beta)$  are always unity, and the projected energy  $E_{J=0}$  will be identically the same as the spherical BCS energy minimum. The composition of  $a_J^2$  will be unity for the  $J=0$  state and zero for all the other states.

Isotopes for which  $E'(\beta) \geq 1$  fall into the third

TABLE IV. Calculated self-consistent energy ( $E = \langle \Phi | H | \Phi \rangle$ ), ground-state energy with respect to  $E$ , i.e., ( $E_{J=0} - E$ ), and the percentage distribution of angular momentum ( $a_J^2$ ) in the deformed intrinsic states of even Ti, Cr, and Fe isotopes for the KBRME for the HJ interaction. All the energies are given in MeV.

Isotope	Type of wave function	$\langle \Phi   H   \Phi \rangle = E$	$\Delta E = (E_{J=0} - E)$	Percentage of $a_J^2$ in the wave function $\Phi$				
				$J=0$	$J=2$	$J=4$	$J=6$	$J=8$
<sup>44</sup> Ti	HF(P)	-28.600	-2.312	6.040	24.844	29.876	22.736	11.628
<sup>46</sup> Ti	HFB(P)	-50.760	1.736	6.299	25.826	29.901	21.687	10.982
<sup>48</sup> Ti	HFB(P)	-70.630	-2.404	8.185	31.341	31.993	19.103	7.214
<sup>50</sup> Ti	HFB(P)	-89.430	-1.587	9.562	34.394	32.089	17.043	5.584
<sup>48</sup> Cr	HFB(P)	-63.250	-1.708	5.634	23.785	28.834	22.321	12.379
<sup>50</sup> Cr	HFB(P)	-86.960	-1.528	5.370	22.832	28.154	22.936	13.000
<sup>52</sup> Cr	HFB(P)	-109.090	-2.078	5.369	22.853	28.228	22.503	12.991
<sup>54</sup> Cr	HFB(P)	-128.760	-2.605	6.546	26.813	30.343	21.184	10.315
<sup>52</sup> Fe	HFB(P)	-100.310	-2.171	3.880	17.284	23.743	22.378	16.267
<sup>54</sup> Fe	HFB(P)	-125.520	-1.883	4.510	19.664	25.730	22.548	14.936
<sup>56</sup> Fe	HFB(P)	-148.110	-1.753	5.257	22.420	27.848	22.461	13.252
<sup>58</sup> Fe	HFB(P)	-168.690	-2.747	7.724	30.152	31.077	19.318	8.346
<sup>58</sup> Fe	HFB(O)	-168.690	...	...	...	...	...	...

group. For such cases the numerator in Eq. (8) for  $J=0$  will always be less than the denominator and therefore  $E_{J=0} < E_{\text{BCS}}$ . The projected spectra will therefore be characterized with the  $J=0$  state lying above the self-consistent energy minimum and the higher  $J$  states lying below the  $J=0$  state. Such a spectrum is physically unacceptable. The only deformed solutions of this type which confronted in the present calculation correspond to  $^{58}\text{Fe}$  (oblate) for both the interactions. In these cases the results were verified by checking the degeneracy of the rotated solution by calculating its self-consistent energy.

### C. Projected Energy Spectra

The projected spectra of the even Ti, Cr, and Fe isotopes corresponding to the prolate-deformed intrinsic shapes are compared with the known experimental results in Figs. 3–5, and the percentage distribution of the angular momentum in the deformed intrinsic states are listed in Tables III and IV. In Figs. 3–5, the positions of the higher angular momentum states are drawn relative to the ground state  $J=0^+$  for each isotope and the ground-state energies corresponding to the  $J=0^+$  state ( $E_{J=0}$ ) for the various isotopes are shown in Table V, and compared with experiment. Since for  $^{50}\text{Ti}$ ,  $^{52}\text{Cr}$ , and  $^{54}\text{Fe}$ , the CY interaction gave spherical BCS solutions, the energy levels for this interaction are obtained from a somewhat less bound (as compared to the spherical BCS solution) HF wave functions having prolate deformation. It can, however, be seen that for these isotopes

the ground-state energy  $E_{J=0}$  is larger than the corresponding spherical BCS energy shown in Table III. In the following, an element-by-element discussion of the results is presented.

### Ti Isotopes

It is evident from Fig. 3 that for  $^{44}\text{Ti}$  there is very good agreement between the projected spectra for both the interactions though the agreement with the known  $2^+$  and  $4^+$  levels is only qualitative. A comparison of the projected spectrum from the HJ interaction with the shell-model calculation of Bhatt and McGrory<sup>13</sup> shows quite good agreement for the  $6^+$  and  $8^+$  levels, but the  $2^+$  level is somewhat more bound in the present calculation. It should be pointed out that the shell-model calculation had been performed by taking the same single-particle energies for both neutrons and protons while they are, as in Ref. 1, taken to be different in this work. Consequently, the validity of such a comparison may be questioned. However, it should be emphasized that as long as the relative differences in the single-particle energies for neutron and proton are not drastically different, a projection calculation using the same single-particle energies for both particles will not give significantly different results. A discussion on the  $Z < N=28$  even isotopes is given later in this section.

### Cr Isotopes

The calculated and observed spectra of even Cr isotopes are shown in Fig. 4. To the knowledge

TABLE V. Comparison of the ground-state energy  $E_{J=0}$  for the CY interaction and KBRME for the HJ interaction with the experimental binding energy relative to the  $^{40}\text{Ca}$  core. The Coulomb correction due to the extracore protons is made according to the prescription described in Ref. 1. The energies are given in MeV.

Isotope	$E_{J=0}$	CY		KBRME		Experimental binding energy with respect to $^{40}\text{Ca}$ core
		$E_{J=0}$ with Coulomb correction	$E_{J=0}$	$E_{J=0}$ with Coulomb correction	$E_{J=0}$	
$^{44}\text{Ti}$	-30.32	-29.66	-30.91	-30.52	-33.53	
$^{46}\text{Ti}$	-51.70	-51.04	-52.50	-51.84	-56.13	
$^{48}\text{Ti}$	-72.08	-71.43	-73.03	-72.38	-76.64	
$^{50}\text{Ti}$	-89.25	-88.61	-91.02	-90.38	-95.73	
$^{48}\text{Cr}$	-60.73	-58.09	-64.96	-62.32	-69.66	
$^{50}\text{Cr}$	-83.14	-80.54	-88.49	-85.89	-92.99	
$^{52}\text{Cr}$	-104.41	-101.84	-111.17	-108.60	-114.29	
$^{54}\text{Cr}$	-125.53	-122.99	-131.37	-128.83	-131.95	
$^{52}\text{Fe}$	-95.71	-89.83	-102.48	-96.60	-105.63	
$^{54}\text{Fe}$	-119.87	-114.07	-127.40	-121.60	-129.69	
$^{56}\text{Fe}$	-143.30	-137.57	-149.86	-144.13	-150.20	
$^{58}\text{Fe}$	-162.35	-156.68	-171.44	-165.77	-167.89	

of the authors there are no excited states known for  $^{48}\text{Cr}$ . It is worth pointing out that for  $^{50}\text{Cr}$  the experimental levels obey the relationship

$$E_J = E_0 + AJ(J+1) + B[J(J+1)]^2, \quad (33)$$

where  $A$  and  $B$  determined from a least-square fit are found to be  $A=0.134$  MeV, and  $B=-0.0014$  MeV. The projected spectrum for the HJ interaction, though only in qualitative agreement with experiments, has a purely rotational structure with  $A=0.043$  MeV and  $B=0.0$ . For  $^{52}\text{Cr}$ , and  $^{54}\text{Cr}$  as well, the HJ interaction gives spectra which exhibit quite a bit of rotational character, but this trend is not observed experimentally. For  $^{52}\text{Cr}$  better agreement is obtained with the CY interaction. Shell-model calculations by Barman Roy, Raj, and Rustgi,<sup>14</sup> and Rustgi *et al.*<sup>15</sup> assuming a  $^{48}\text{Ca}$  core and employing the HJ interaction also give improved agreement for this isotope than obtained here.

#### Fe Isotopes

The calculated and experimental spectra of even Fe isotopes are shown in Fig. 5. It is seen that the projected spectra of  $^{52}\text{Fe}$ ,  $^{54}\text{Fe}$ , and  $^{56}\text{Fe}$  for the HJ interaction, show rotational structure, favoring the same value of the parameter  $A$  in Eq. (33) for  $^{52}\text{Fe}$  and  $^{54}\text{Fe}$  as the one for  $^{50}\text{Cr}$ , but  $A=0.0475$  MeV for  $^{56}\text{Fe}$ . The projected spectra of  $^{58}\text{Fe}$  for the prolate HFB solutions differ drastically for the two interactions which follow from the criteria involving  $E'(\beta)$  discussed earlier.

#### D. Percentage Admixture of Good Angular Momentum States in the Deformed Wave Function

A comparison of the percentage admixture of good angular momentum states can be made with the help of Tables III and IV. For  $^{44}\text{Ti}$ , both the interactions show striking similarity in  $a_{J^2}$ . However, this behavior changes slowly and becomes significantly different for  $^{50}\text{Ti}$  as for this isotope the self-consistent solution for the CY interaction is taken to be HF whereas for the HJ interaction it is deformed BCS.

For  $^{48}\text{Cr}$  both the interactions give similar composition of the different angular momentum states in the deformed wave function. A similarity of the wave functions for this isotope is also evident from a comparison of the pickup strengths in various single-particle states.<sup>1</sup> However, for  $^{54}\text{Cr}$  the pickup strengths for both the interactions differ significantly even though the percentage admixture composition is strikingly similar.

From Table IV it is also seen that for the HJ interaction with the increase in the number of

neutrons, the percentage composition of the  $J=0$  state increases but decreases for the  $J=8$  state.

#### E. Ground-State Energy in the $J=0$ State

It is customary to compare the binding energy of a nuclear system with the self-consistent energy minimum after applying a correction for the Coulomb repulsion amongst the extracore protons. However, for a deformed structure, energy of the projected  $J=0$  state rather than the self-consistent energy, should be used for comparison. In the present calculation, a depression of the  $J=0$  ground state relative to the respective self-consistent energy minimum ( $E = \langle \Phi | H | \Phi \rangle$ ) is given in Tables III and IV and the comparison of the ground-state energy in the  $J=0$  state with Coulomb correction and experimental binding energies is made in Table V. An attempt is made to understand the behavior of this lowering of the  $J=0$  state in terms of its percentage mixture together with the structure of the projected spectrum. To achieve this, for an axially symmetric system, one can write for the depression in energy

$$\begin{aligned} \Delta E &= E_{J=0} - E = E_{J=0}(1 - a_{J=0}^2) - E' \sum_{J \neq 0} a_J^2 \\ &= (E_{J=0} - E')(1 - a_{J=0}^2), \end{aligned} \quad (34)$$

where

$$E' = \frac{\sum_{J \neq 0} a_J^2 E_J}{\sum_{J \neq 0} a_J^2}, \quad (35)$$

and

$$\sum_{J \neq 0} a_J^2 = (1 - a_{J=0}^2). \quad (36)$$

On approximating  $E'$  by  $E_{J=2}$ , one can get an upper limit for  $\Delta E$ , i.e.

$$\Delta E < (E_{J=0} - E_{J=2})(1 - a_{J=0}^2). \quad (37)$$

An exact calculation employing Eq. (35) and Tables III and IV shows that  $E'$  usually lies considerably higher than the energy of the  $J=2$  state. Consequently  $(E_{J=0} - E')$  in Eq. (34) is quite large as compared to  $|E_{J=0} - E_{J=2}|$ .

One can now apply these considerations to  $^{54}\text{Fe}$  in Fig. 5. From this figure it is clear that with respect to the HJ interaction the spectrum for the CY interaction is much spread out. It is, therefore, expected that in comparison with the HJ spectrum  $E'$  for the CY spectrum will be much higher than  $E_{J=2}$ . However, from Tables III and IV it is seen that the magnitude of  $\Delta E$  for the HJ interaction is larger than that for the CY interaction. This is so because the much larger percentage composition of  $a_{J^2}$  in the  $J=0$  state for the CY interaction decreases the second term on

the right side in Eq. (34) causing a reduction in  $\Delta E$ .

From Table V it is evident that for all the Ti, Cr, and Fe isotopes, the calculated ground-state energies in the  $J=0^+$  state, when corrected for the Coulomb interaction, are quite close to the experimental numbers, for both the interactions. The numbers for the HJ interaction are, however, found to show slightly better agreement. As pointed out in Ref. 1, this is not surprising, since the  $T=1$  force in the HJ interaction is somewhat stronger than in the CY interaction. It may also be pointed out that the agreement is improved for both the interactions in the present case over that obtained in Ref. 1, where the comparison was made directly with the self-consistent energy  $\langle \Phi | H | \Phi \rangle$  rather than with  $E_{J=0}$ , which has some additional binding  $\Delta E$ , as described above.

#### F. $Z < N = 28$ Nuclei with the CY Interaction

It has been pointed out earlier that the self-consistent HFB calculation with the CY interaction yields spherical BCS shape for  $^{50}\text{Ti}$ ,  $^{52}\text{Cr}$ , and  $^{54}\text{Fe}$  isotopes but their prolate HF minima lie only slightly higher in energy; 0.3 MeV for  $^{50}\text{Ti}$ , 0.9 MeV for  $^{52}\text{Cr}$ , and 0.8 MeV for  $^{54}\text{Fe}$ . It is, therefore, quite pertinent to examine the  $J=0$  state projected from these HF wave functions to see if they fall below their BCS minima. From Table III it is clear that this is true for all the three isotopes. Since the projected spectra agree well with experiments particularly for the  $2^+$  state, it is therefore essential to calculate the other properties for these isotopes to decide in favor of one of the solutions. The  $2^+$  states calculated employing spherical BCS solutions and random-phase approximation also agree rather well with experiments.<sup>16</sup> The pickup strengths for neutrons and protons from the BCS and deformed HF wave functions also hardly differ,<sup>17</sup> making a choice between the two solutions very different. A possible way out is to examine the spin of the odd-proton system. This can be easily accomplished if the even  $Z < N = 28$  nucleus is regarded as a spherical system and the unpaired particle is put in the lowest partially occupied single-particle state. It is found that, in agreement with a detailed calculation<sup>18</sup> the spherical BCS solutions explain the spins of  $^{51}\text{V}$ ,  $^{53}\text{Mn}$ , and  $^{55}\text{Co}$ , but the deformed HF solutions fail to do so.

#### IV. CONCLUSIONS

In the preceding section we have presented the results of calculations of the even Ti, Cr, and Fe isotopes in terms of the projection method.

It may be pointed out that the projection procedure described in Sec. II is equally useful for deformed HF and deformed BCS solutions. In Sec. III, a specific criterion for the applicability of the projection method is given. From the discussion of the projected spectra in Sec. III, it is clear that the agreement with experiments varies from quantitative in some cases to qualitative in most cases. It is also noticed from a comparison of the projected spectra for the CY and HJ interactions that they quite often differ. These differences may be attributed to the differences in the two-body matrix elements of the two interactions. For example a comparison of the matrix elements of the form  $\langle jj_\lambda | V_A | jj_\lambda \rangle_{JT}$  in the  $j = \frac{7}{2}$  and  $j_\lambda = \frac{7}{2}$  states shows that for  $T=0$  and  $J=1, 3, 5$ , and  $7$ , they are more attractive for the CY interaction as compared to the Kuo-Brown renormalized matrix elements (KBRME); for  $T=1$  and  $J=0$  and  $2$ , the KBRME are somewhat more attractive whereas for  $J=4$  it is the CY interaction which is more attractive. Similarly it is found that for  $j = \frac{5}{2}$ , the matrix elements for the HJ interaction are more attractive for  $T=0$  and  $J=2, 4$ , and  $6$  in comparison with their counterparts for the CY interaction, but for  $J=1, 3, 5$ , and  $7$  the matrix elements are almost equal for both the interactions. For  $T=1$ , and  $J=1$  and  $2$ , the CY interaction is more repulsive. A similar comparison for  $j = \frac{1}{2}$  and  $j_\lambda = \frac{7}{2}$  and  $j = \frac{3}{2}$  and  $j_\lambda = \frac{7}{2}$  matrix elements and others accounts for most of the differences in the spectra. The close agreement in the level spectrum of  $^{44}\text{Ti}$  is essentially due to the similarity of the two wave functions and the effect of the differences in the interaction show up only moderately in the higher states. For  $^{50}\text{Cr}$ , the HJ interaction gives a purely rotational spectrum but it is only in qualitative agreement with experiment. The spectra with characteristic rotational features were also obtained for many Fe isotopes for the HJ interaction. The fact that the projected spectra are sensitive to interactions makes one hopeful of obtaining better results with improved matrix elements calculated with realistic nucleon-nucleon potentials.

#### ACKNOWLEDGMENTS

The authors are grateful to Professor Gregory Breit for interesting discussions.

Thanks are due the staff of the Computing Center of the State University of New York at Buffalo for providing the machine time. A grant-in-aid from the Research Foundation of the State University of New York to one of the authors (MLR) is also gratefully acknowledged.

\*On leave from Saha Institute of Nuclear Physics, Calcutta, India.

<sup>1</sup>H. Chandra and M. L. Rustgi, Phys. Rev. C **3**, 1476 (1971).

<sup>2</sup>T. T. S. Kuo and G. E. Brown, Nucl. Phys. **A114**, 241 (1968).

<sup>3</sup>R. E. Peierls and J. Yoccoz, Proc. Phys. Soc. (London) **A70**, 381 (1957).

<sup>4</sup>W. H. Bassichis, B. Giraud, and G. Ripka, Phys. Rev. Letters **15**, 980 (1965).

<sup>5</sup>C. S. Warke and M. R. Gunye, Phys. Rev. **155**, 1084 (1967); M. Bouten, P. Van Leuven, H. Depuydt, and L. Schotsmans, Nucl. Phys. **A100**, 90 (1967).

<sup>6</sup>G. Ripka, in *Advances in Nuclear Physics*, edited by M. Baranger and E. Vogt (Plenum, New York, 1968), Vol. 1.

<sup>7</sup>N. Onishi and S. Yoshida, Nucl. Phys. **80**, 367 (1966).

<sup>8</sup>K. R. Sandhya Devi, S. B. Khadkikar, J. K. Parikh,

and B. Banerjee, Phys. Letters **32B**, 179 (1970).

<sup>9</sup>R. Beck, H. J. Mang, and P. Ring, Z. Physik **231**, 26 (1970).

<sup>10</sup>M. E. Rose, *Elementary Theory of Angular Momentum* (Wiley, New York, 1957), p. 52.

<sup>11</sup>H. Chandra and M. L. Rustgi, Phys. Rev. C **5**, 1791 (1972).

<sup>12</sup>B. F. Bayman, Nucl. Phys. **15**, 33 (1960).

<sup>13</sup>K. H. Bhatt and J. B. McGrory, Phys. Rev. C **3**, 2293 (1971).

<sup>14</sup>B. Barman Roy, R. Raj, and M. L. Rustgi, Phys. Rev. C **1**, 207 (1970).

<sup>15</sup>M. L. Rustgi, R. P. Singh, B. Barman Roy, R. Raj, and C. C. Fu, Phys. Rev. C **3**, 2238 (1971).

<sup>16</sup>H. Chandra, Phys. Rev. **185**, 1320 (1969).

<sup>17</sup>H. Chandra, Phys. Rev. C **2**, 2444 (1970).

<sup>18</sup>R. Raj, M. L. Rustgi, and R. P. Singh, Phys. Rev. **181**, 1536 (1969).

## Level Structure of <sup>48</sup>Ti for $E_x < 3.5$ MeV\*

T. T. Bardin, J. A. Becker, and T. R. Fisher

Lockheed Palo Alto Research Laboratory, Palo Alto, California 94304

(Received 4 August 1972)

The reactions <sup>48</sup>Ti( $p, p'$ ), <sup>48</sup>Ti( $\alpha, \alpha'$ ), <sup>48</sup>Ti(<sup>35</sup>Cl, <sup>35</sup>Cl'), and <sup>48</sup>V( $\beta^+$ ) have been employed to measure excitation energies, lifetimes, and  $\gamma$ -decay branching ratios for <sup>48</sup>Ti levels with  $E_x < 3.5$  MeV. The results for excitation energies (in keV) and corresponding lifetimes (in psec) are: 983.35 $\pm$ 0.10, 6.0 $\pm$ 1.3; 2295.5 $\pm$ 0.15, 2.4 $\pm$ 0.6; 2420.3 $\pm$ 0.15, 0.035 $\pm$ 0.007; 2997.4 $\pm$ 0.25, 0.160 $\pm$ 0.032; 3223.5 $\pm$ 0.20, 0.042 $\pm$ 0.014; 3239.7 $\pm$ 0.35, 0.044 $\pm$ 0.018; 3358.7 $\pm$ 0.65, 0.350 $\pm$ 0.087; 3370.7 $\pm$ 0.30, 0.018 $\pm$ 0.007. Reduced electromagnetic-transition matrix elements have also been derived from the data. No evidence is found for a doublet at an energy of 3.224 MeV. The previous data on the 3.224-MeV level are reexamined in the light of the present results, and the tentative assignment  $J^\pi = 3^+$  is consistent with all data. A tentative assignment of  $J^\pi = 4^+$  is given to the level at 3.240 MeV. The present results are in reasonable agreement with the predictions of a model in which the valence nucleons are confined to the  $f_{7/2}$  orbital.

### I. INTRODUCTION

The first comprehensive attempt to explain the properties of nuclei in the  $f_{7/2}$  shell was the calculation of McCullen, Bayman, and Zamick (MBZ).<sup>1</sup> These authors considered a model in which the extracore nucleons were confined entirely to the  $f_{7/2}$  shell, and level spectra were computed using matrix elements for the residual two-body interaction derived from the experimental spectrum of <sup>42</sup>Sc. Many of the general features of the nuclei considered were well reproduced by the model, although the number of experimental levels was generally greater than the predicted number. MBZ also pointed out an interesting feature of the wave functions for a nucleus such as <sup>48</sup>Ti, which is its own cross-conjugate: the wave functions are either even or odd under the interchange of protons and

neutron holes. This property sometimes produces two levels of the same spin which lie close together in energy, and explains the close juxtaposition of two 6<sup>+</sup> levels near 3.5-MeV excitation energy in <sup>48</sup>Ti.

A further consequence of this odd-even property, sometimes called the signature of the wave function, has been discussed by Lawson.<sup>2</sup> The  $E2$  transition matrix element connecting two such levels is proportional to  $e_p \pm e_n$ , where  $e_p$  and  $e_n$  are the proton and neutron effective charges; the plus sign applies if the levels have opposite signature, and the minus sign applies if the signatures are the same. To a good approximation,  $e_p - e_n$  should be equal to  $e$ , the free proton charge, even in the presence of core polarization effects.<sup>2</sup> Thus, measurement of  $E2$  transition matrix elements between levels of the same signature provides a sensitive